ChemComm

COMMUNICATION

View Article Online
View Journal | View Issue

Cite this: *Chem. Commun.*, 2023, **59**, 10556

Received 4th April 2023,
Accepted 3rd August 2023

DOI: 10.1039/d3cc01662e

rsc.li/chemcomm

Ferromagnetism induced by in-plane strain in a bulk VS_2-based superlattice: $(LiOH)_{0.1}VS_2$†

Ruijin Sun, *[a] Jun Deng,[b] Yuxin Ma,[b] Munan Hao,[b] Xu Chen,[b] Dezhong Meng,[a] Changchun Zhao,[a] Shixuan Du,[b] Shifeng Jin*[b] and Xiaolong Chen *[b]

Transition metal dichalcogenides (TMDs) have attracted intensive research interest due to their diverse properties. However, ferromagnetism is not observed in layered TMDs, except for monolayer VSe_2. In this study, we report the synthesis of a bulk ferromagnetic material $(LiOH)_{0.1}VS_2$ based on topochemical reactions. The results demonstrate that the $(LiOH)_{0.1}VS_2$ crystal exhibits strong anisotropic ferromagnetism below a critical temperature of 40 K. Calculations uncover that the in-plane strains in a $\sqrt{3} \times \sqrt{7}$ VS_2 superlattice can induce large magnetic anisotropic energy, which stabilizes the long-range ferromagnetic order. The findings provide a new approach to induce ferromagnetism in bulk TMD materials.

TMDs, as a large family of layered van der Waals (vdW) materials of general formula MX_2 (M = metals, X = chalcogens), have been the subject of intensive research due to their rich properties that make them attractive for both fundamental studies of novel physical phenomena and for practical applications.[1–3] With the merits of adjustable structural phase and layer thickness and especially the highly tunable chemical compositions in both the M and X sites, TMDs can display a wide range of electronic properties, such as optoelectronic properties and luminance (*e.g.*, MoS_2, WS_2),[4–6] charge density waves and superconductivity (*e.g.*, $NbSe_2$ and TaS_2),[7–9] and valleytronic properties with a controllable valley degree of freedom (*e.g.*, MoS_2, WSe_2).[10] However, this family has been missing one crucial member: ferromagnets.[11–14] It is only recently that ferromagnetism has been experimentally observed in atomic thick VSe_2 films, and the findings are still debatable. Until now, there has been no experimental success in inducing ferromagnetism in bulk TMD-based materials.

To induce intrinsic ferromagnetism in TMDs, the M site of the MX_2 material must be occupied by high-spin state atoms.[15] The only M element that, in its high spin state, can meet the requirements for chemical stability and the formation of a layered structure in TMDs is vanadium (V). With the 1T structural configuration and high-spin state of M element V, bulk VX_2 (X = S, Se) is experimentally determined to be paramagnetic,[16,17] but it is theoretically proposed to exhibit ferromagnetic order down to the monolayer limit.[18–20] Recent studies by M. Bonilla *et al.* reported the observation of a ferromagnetic state up to room temperature in monolayer VSe_2.[21] Later, several similar experiments failed to reproduce the ferromagnetism in monolayer VSe_2, making the findings a matter of debate.[22–27] For instance, the results of ARPES on monolayer VSe_2 show that there are no exchange-split electronic bands and ferromagnetically coupled V atoms down to 10 K.[22] It is also reported based on the results of STM/nc-AFM that ferromagnetism does exist in the VSe_2 monolayer, but only in the region with abundant Se-defects,[25,26] suggesting that the observed ferromagnetism should not be intrinsic. Theoretically, it is proposed that intrinsic ferromagnetic order can be stabilized in the strained VS_2/VSe_2 monolayer, wherein both the magnetic moments and strength of magnetic coupling increase rapidly with increasing isotropic strain.[19] Given these conflicting experimental and theoretical results, we aim to fabricate a bulk V-based TMD material that is free of abundant defects, wherein intrinsic ferromagnetism may be induced in the strained VS_2/VSe_2 lattice.

In this study, we report the successful realization of ferromagnetism in a bulk superlattice $(LiOH)_{0.1}VS_2$, which is constructed based on paramagnetic 1T-VS_2. To ensure the VS_2 layer is free of the defects that generally occurred in samples synthesised at high temperatures, the title compound is obtained through a low temperature topochemical reaction. $K_{0.6}VS_2$ single crystal, which is known to have defect-free T-VS_2 layers,[28] is used as the parent matrix. The structural solution of a $(LiOH)_{0.1}VS_2$ single crystal and maxim entropy charge density analysis revealed a $\sqrt{3} \times \sqrt{7}$ commensurate superlattice in stoichiometric VS_2 layers, suggesting that in-plane strains are imposed to the VS_2 matrix through insertion of hydrate layers. Magnetic properties measurement revealed that below ~40 K, the bulk material becomes a ferromagnet with significant magneto-crystalline anisotropy. Extensive

[a] *School of Science, China University of Geosciences, Beijing (CUGB), Beijing, 100083, China. E-mail: srj@cugb.edu.cn*
[b] *Institute of Physics, Chinese Academy of Science, Beijing, 100190, China*

† Electronic supplementary information (ESI) available. CCDC. 2241083. For ESI and crystallographic data in CIF or other electronic format see DOI: https://doi.org/10.1039/d3cc01662e

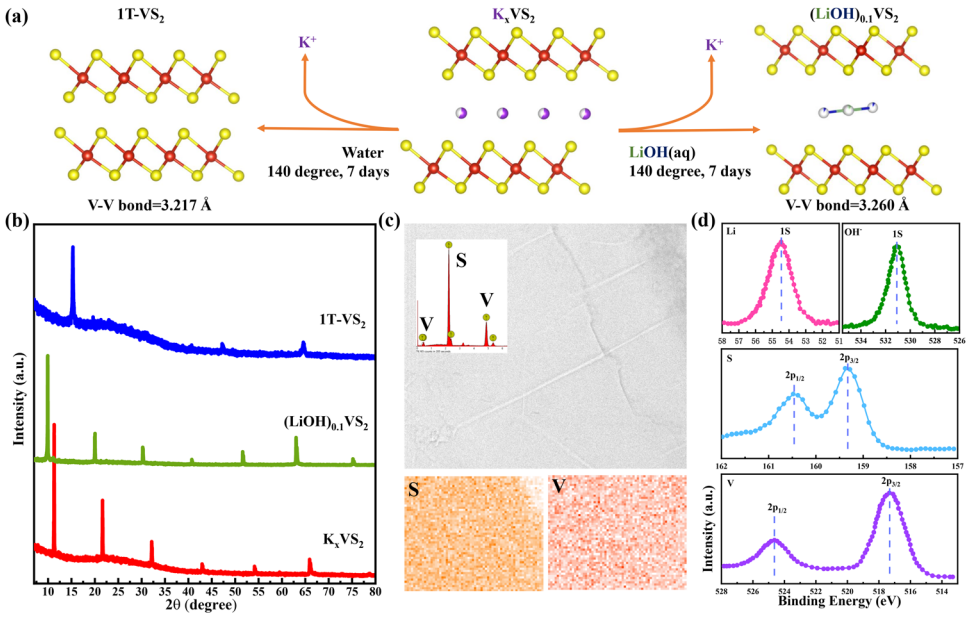

Fig. 1 (a) Reaction scheme for the manipulation of $(LiOH)_{0.1}VS_2$ and 1T-VS_2. (b) Powder X-ray diffraction patterns along the (00l) direction of products $(LiOH)_{0.1}VS_2$ and 1T-VS_2 and the matrix K_xVS_2 single crystals. (c) SEM image and EDS compositional mapping of $(LiOH)_{0.1}VS_2$. (d) XPS pattern of V 2p, S 2p, Li 1s, and O 1s (OH^-) in $(LiOH)_{0.1}VS_2$.

density functional theory (DFT) calculations are also applied to uncover the origin of the emergence of ferromagnetism in stoichiometric VS_2 layers.

The topochemical reaction starting from the $K_{0.6}VS_2$ single crystalline matrix to $(LiOH)_{0.1}VS_2$ and 1T-VS_2 is demonstrated in Fig. 1a. The as-prepared $(LiOH)_{0.1}VS_2$ single crystal was characterized by powder X-ray diffraction (PXRD). As shown in Fig. 1b, after 7 days of reaction in the LiOH aqueous solution, the (00l) reflections of the $K_{0.6}VS_2$ precursors are completely replaced by a new set of ones that systematically shift to lower angles, which indicates the presence of new intercalated species in between the VS_2 layers. The chemical stoichiometry of the starting material $K_{0.6}VS_2$ is determined by scanning electron microscopy (SEM) and energy-dispersive X-ray spectroscopy (EDS) mapping (Fig. S1, ESI†). The homogeneous distribution of V and S with a molar ratio of 1 : 2 is also confirmed by EDS in $(LiOH)_{0.1}VS_2$, as shown in Fig. 1c. X-ray photoelectron spectroscopy (XPS) analysis was used to identify the species and oxidation states of elements such as Li, OH^-, V, and S, in $(LiOH)_{0.1}VS_2$. As shown in Fig. 1d, the Li 1s (55 eV) and O 1s (531 eV) peaks appeared in $(LiOH)_{0.1}VS_2$, which are identical to the reported LiOH spectra, suggesting the insertion of LiOH groups.[29] Moreover, only one kind of XPS peak of V 2p (517 and 525 eV) and S 2p (159.5 and 160.5 eV) was detected in $(LiOH)_{0.1}VS_2$, with their peak positions consistent with the stoichiometric 1T-VS_2, suggesting that after reaction the VS_2 layer becomes charge neutral and there is basically no V transferred to the interlayer space.[30] From this, we can conclude that VS_2 layers are inserted by charge-neutral groups LiOH. The calculated Li : OH^- : V : S atomic ratio from XPS data (0.1 : 0.1 : 1 : 2) is in agreement with the results of ICP-AES in Table S1 (ESI†), suggesting that the material has good lateral uniformity and that a trace amount of LiOH molecules is incorporated in-between the VS_2 layers.

We then used single-crystal X-ray diffraction (SXRD) to determine the crystal structure of $(LiOH)_{0.1}VS_2$. The SXRD data can be indexed by a $P\bar{1}$ unit cell, with lattice parameters a = 5.6557(6) Å, b = 8.6279(2) Å and c = 9.0551(7) Å. To probe the light elements of Li, O and H, high precision electron density distributions (EDD) of $(LiOH)_{0.1}VS_2$ (wR_F = 0.021) were constructed based on the model independent maximum-entropy method (MEM).[31] It's clearly shown that in-between the VS_2 layers, there are two sites with charge aggregation (Fig. 2a). Considering that the XPS data suggest no noticeable interlayer V ions, it is reasonable to ascribe the heavier charge aggregation to O and the lighter one to Li. Subsequent refinement on the occupancy of O & Li leads to a value close to the formula determined by chemical analysis. As shown in Fig. 2b, the interlayer LiOH exists in molecular form with straight rod-like shape, similar to the previous findings.[32,33] Intriguingly, the VS_2 layer in $(LiOH)_{0.1}VS_2$ forms a $\sqrt{3} \times \sqrt{7}$ ($\sqrt{3} \times 3.26 = 5.65$, $\sqrt{7} \times 3.26 = 8.63$) super cell in comparison with hexagonal 1T-VS_2. The V–V bond length (3.260 Å) is approximately 1.2% longer than bulk 1T-VS_2, suggesting that the insertion of LiOH molecules applies ~1.2% tensile strain to the host layer. The [VS_6] polyhedron is also distorted, resulting in three inequivalent V–S bond lengths (Fig. 2c). The large anisotropic in-plane strain and a decrease in crystal symmetry caused by the insertion of molecules are also observed in some FeSe intercalated compounds.[34] The refined crystal structural data is shown in Tables S2 (ESI†), and the bond lengths and angles for $(LiOH)_{0.1}VS_2$ are deposited in Table S3 (ESI†).

Magnetic properties of the $(LiOH)_{0.1}VS_2$ single crystals were investigated using a PPMS-VSM system. Fig. 3a and b show the magnetic moment against the magnetic field (M–H) curves measured at different temperatures with the field parallel and perpendicular to the crystal. The M–H hysteresis loops observed

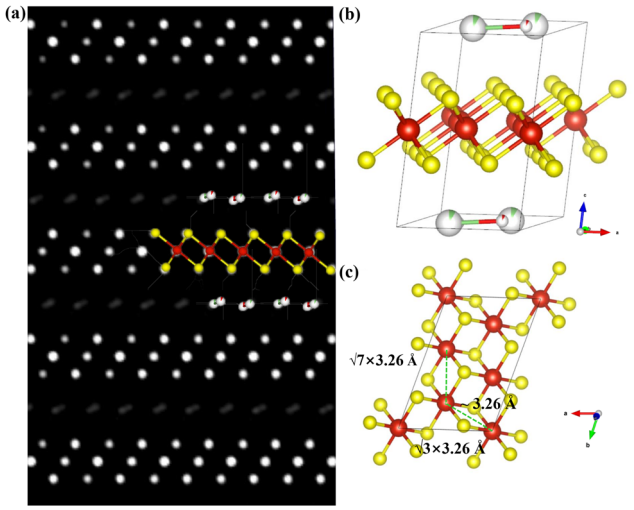

Fig. 2 (a) Charge density map for $(LiOH)_{0.1}VS_2$. (b) Structure model for $(LiOH)_{0.1}VS_2$. (c) Scheme for the $\sqrt{3} \times \sqrt{7}$ superlattice in $(LiOH)_{0.1}VS_2$.

at 10 K well demonstrate the ferromagnetism in $(LiOH)_{0.1}VS_2$, while both the as-grown 1T-VS_2 and $K_{0.6}VS_2$ are paramagnetic (Fig. S2 and S3, ESI†). Notably, the in-plane hysteresis loop is significantly larger than the out-of-plane one, indicating the strong anisotropy of ferromagnetism. The easy axis in $(LiOH)_{0.1}VS_2$ is parallel to the *xy* plane, which is in line with the findings in the VSe_2 monolayer.[21] Moreover, the small coercivity field (200 Oe) suggests that $(LiOH)_{0.1}VS_2$ is a soft magnet material, which is also similar to monolayer VSe_2.[21] Fig. 3c shows the zero-field cooling (ZFC) and field cooling (FC) curves with in-plane and out-of-plane fields. The magnetic moments decrease with increasing temperature and both vanish at around 40 K. This behavior again verifies the existence of ferromagnetic order in $(LiOH)_{0.1}VS_2$. Fig. 3d shows

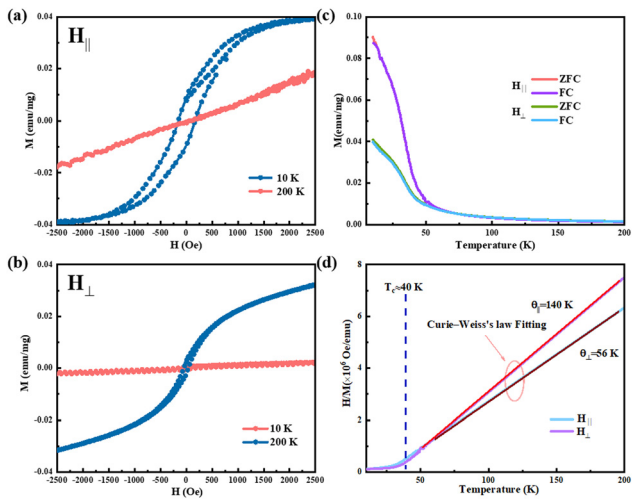

Fig. 3 (a) *M*–*H* loops obtained with an in-plane magnetic field at 10 K and 200 K. (b) *M*–*H* loops obtained with an out-of-plane magnetic field at 10 K and 200 K. (c) The field cooling (FC) and zero-field cooling (ZFC) curves obtained with an in-plane and an out-of-plane magnetic field of 1 T. (d) *H*/*M versus* temperature curves, showing the ferromagnetic transition at $T_c \approx 40$ K.

the corresponding temperature-dependent inverse *M*–*T* curve. Obviously, the ferromagnetic–paramagnetic (FM–PM) transition occurs at a critical temperature (T_c) of about 40 K. We found that both the in-plane and out-of-plane high-temperature (>50 K) data can be well fitted by Curie–Weiss's law,

$$\chi(T) = \frac{C}{T - \theta},$$

where θ and C are the Weiss and the Curie constants. The fitting yields a θ of 140 K for in-plane and 56 K for out-of-plane fields, respectively. Such a large difference in θ suggests the anisotropic paramagnetic behavior of the $(LiOH)_{0.1}VS_2$. This behavior, along with the anisotropic *M*–*H* data in the ferromagnetic state, confirms the existence of strong magneto-crystalline anisotropy.

To gain an in-depth understanding, we performed DFT calculations to reveal the origin of the ferromagnetic orders in $(LiOH)_{0.1}VS_2$. We first compared the magnetic ground states of $(LiOH)_{0.1}VS_2$ and bulk 1T-VS_2 and found that both have ferromagnetic ground states (as shown in Fig. S4 and S5, ESI†). For long-range magnetism in 2D systems, the magnetic anisotropy energy (MAE) plays an important role in stabilizing the ferromagnetism at finite temperatures.[35–37] Fig. 4a shows the angular dependent MAE, which is evaluated by rotating the spin of V atoms in the *xy* and *xz* planes. The MAEs show that MAE of both $(LiOH)_{0.1}VS_2$ and 1T-VS_2 are nearly isotropic in the xy plane, but are anisotropic in the *xz* plane. The easy axes of both materials are in the *xy* plane. Moreover, the MAE of $(LiOH)_{0.1}VS_2$ (91.88 μeV) is more than three times that of 1T-VS_2 (26.94 μeV), resulting in the long-range ferromagnetism of $(LiOH)_{0.1}VS_2$, which is absent in 1T-VS_2. To further elucidate the origin of the enhancement of MAE in $(LiOH)_{0.1}VS_2$, a set of trial structures are built (Fig. S6, ESI†).

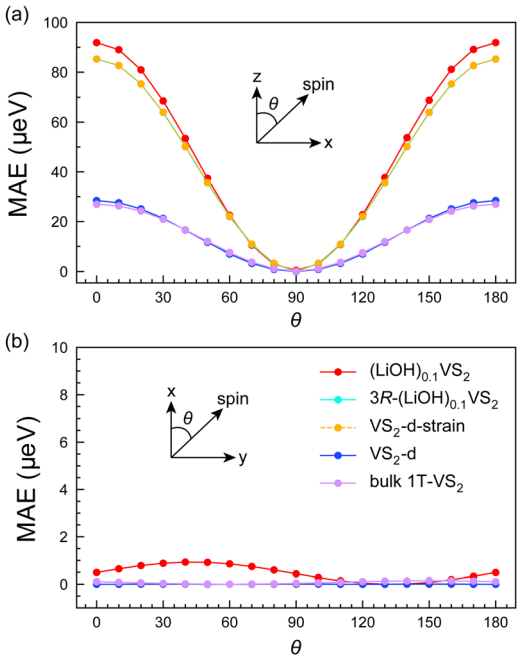

Fig. 4 Angular dependence of magnetic anisotropic energy (MAE) in (a) *xz* and (b) *xy* planes. The definition of the structures can be found in Fig. S6 (ESI†).

Compared with 1T-VS_2, $(LiOH)_{0.1}VS_2$ can be considered as 3R stacking of the $\sqrt{3} \times \sqrt{7}$ superlattice of T-VS_2 layers with larger in-plane lattice constant and interlayer distance (Fig. 4b). Thus, four aspects possibly induce the enhancement of MAE in $(LiOH)_{0.1}VS_2$: in-plane strain, in-plane distortion, interlayer distance, and stacking ordering. Based on 1T-VS_2, three artificial structures are subsequently constructed, as illustrated in Fig. S6 (ESI†). Compared with $(LiOH)_{0.1}VS_2$, VS_2-d has the same interlayer distance, VS_2-d-strain has the same interlayer distance and lattice constant, while 3R-$(LiOH)_{0.1}VS_2$ has the same interlayer distance, lattice constant and stacking ordering. By analyzing their MAEs (Fig. 4), we find that only in-plane tensile strain (the orange line in Fig. 4a) significantly enhances the MAE of VS_2, and in-plane distortion has only a minor influence on MAE, while stacking ordering and interlayer spacing have negligible impacts. Beside the in-plane tensile strain, its also proposed that a large concentration of Se defects may also induce the magnetism in monolayer VSe_2.[25,26] Considering that in $(LiOH)_{0.1}VS_2$, both the chemical analysis data and diffraction analysis have precluded the existence of abundant S vacancies within the resolution limits, the in-plane strain induced magnetism is still the most promising scenario. Moreover, we believe that when we reduce $(LiOH)_{0.1}VS_2$ to a few layers or even a monolayer, it can achieve greater flexibility in controlling the in-plane strain of VS_2 by manipulating factors such as substrate type and defects. This, in turn, holds the potential to realize higher T_c two-dimensional ferromagnetism.

In summary, bulk single crystals of $(LiOH)_{0.1}VS_2$ have been successfully synthesized using the topochemical method, exhibiting intrinsic ferromagnetic ordering with a T_c of $\sim$ 40 K. The occurrence of ferromagnetic order in this $\sqrt{3} \times \sqrt{7}$ VS_2 superlattice provides strong evidence that applying in-plane strain in VS_2/VSe_2-based materials can introduce ferromagnetism. The findings reported here are expected to open the gate to more TMD-based ferromagnets, and will contribute to a better understanding of the emergence of ferromagnetism in 2D TMD materials as well.

This work is financially supported by the Development Program of China (Grants No. 2018YFE0202600) and the National Natural Science Foundation of China (NSFC) (Grants No. 52102338, 51772323, 52171229) and was experimentally supported by the Synergetic Extreme Condition User Facility (SECUF).

Conflicts of interest

There are no conflicts to declare.

Notes and references

1 K. S. Novoselov, D. Jiang, F. Schedin, T. J. Booth, V. V. Khotkevich, S. V. Morozov and A. K. Geim, *Proc. Natl Acad. Sci. U. S. A.*, 2005, **102**, 10451–10453.
2 S. Manzeli, D. Ovchinnikov, D. Pasquier, O. V. Yazyev and A. Kis, *Nat Rev Mater*, 2017, **2**, 17033.
3 J. A. Wilson and A. D. Yoffe, *Adv. Phys.*, 1969, **18**, 193–335.
4 K. F. Mak, C. Lee, J. Hone, J. Shan and T. F. Heinz, *Phys. Rev. Lett.*, 2010, **105**, 136805.
5 A. Splendiani, L. Sun, Y. Zhang, T. Li, J. Kim, C. Y. Chim, G. Galli and F. Wang, *Nano Lett.*, 2010, **10**, 1271–1275.
6 A. Khan, T. Lu, W. Ma, Y. Lu and Y. Liu, *Adv. Electron. Mater.*, 2020, **6**, 1901381.
7 X. Xi, L. Zhao, Z. Wang, H. Berger, L. Forro, J. Shan and K. F. Mak, *Nat. Nanotech*, 2015, **10**, 765–770.
8 S. Kolekar, M. Bonilla, Y. Ma, H. Coy Diaz and M. Batzill, *2D Mater.*, 2017, **5**, 015006.
9 A. W. Tsen, B. Hunt, Y. D. Kim, Z. J. Yuan, S. Jia, R. J. Cava, J. Hone, P. Kim, C. R. Dean and A. N. Pasupathy, *Nat. Phys.*, 2016, **12**, 208–212.
10 J. Schaibley, H. Yu, G. Clark, P. Rivera, J. Ross, K. L. Seyler, W. Yao and X. Xu, *Nat. Rev. Mater.*, 2016, **1**, 16055.
11 K. S. Burch, D. Mandrus and J. G. Park, *Nature*, 2018, **563**, 47–52.
12 B. Huang, G. Clark, E. Navarro-Moratalla, D. R. Klein, R. Cheng, K. L. Seyler, D. Zhong, E. Schmidgall, M. A. Mcguire, D. H. Cobden, W. Yao, D. Xiao, P. Jarillo-Herrero and X. Xu, *Nature*, 2017, **546**, 270–273.
13 B. Huang, G. Clark, D. R. Klein, D. MacNeill, E. Navarro-Moratalla, K. L. Seyler, N. Wilson, M. A. McGuire, D. H. Cobden, D. Xiao, W. Yao, P. Jarillo-Herrero and X. Xu, *Nat. Nanotechnol.*, 2018, **13**, 544–548.
14 Y. Deng, Y. Yu, Y. Song, J. Zhang, N. Z. Wang, Z. Sun, Y. Yi, Y. Z. Wu, S. Wu, J. Zhu, J. Wang, X. H. Chen and Y. Zhang, *Nature*, 2018, **563**, 94–99.
15 X. Jiang, Q. Liu, J. Xing, N. Liu, Y. Guo, Z. Liu and J. Zhao, *Appl. Phys. Rev*, 2021, **8**, 031305.
16 C. F. van Bruggen and C. Haas, *Solid State Commun.*, 1976, **20**, 251–254.
17 M. Bayard and M. J. J. Sienko, *Solid State Chem.*, 1976, **19**, 325–329.
18 Z. L. Popov, *et al.*, *Phys. Chem. Chem. Phys.*, 2016, **18**, 33047–33052.
19 Y. Ma, Y. Dai, M. Guo, C. Niu, Y. Zhu and B. Huang, *ACS Nano*, 2012, **6**, 1695–1701.
20 H. R. Fuh, B. Yan, S. C. Wu, C. Felser and C. R. Chang, *New J. Phys.*, 2016, **18**, 113038.
21 M. Bonilla, S. Kolekar, Y. Ma, H. C. Diaz, V. Kalappattil, R. Das, T. Eggers, H. R. Gutierrze, M. H. Phan and M. Batzill, *Nat. Nanotechnol.*, 2018, **13**, 289–293.
22 J. Feng, D. Biswas, A. Rajan, M. D. Watson, F. Mazzola, O. J. Clark, K. Underwood, I. Markovic, M. Mclaren, A. Hunter, D. M. Burn, L. B. Duffy, S. Barua, G. Balakrishnan, F. Bertran, P. L. Fevre, T. K. Kim, G. Laan, T. Hesjedal, P. Wahl and P. D. C. King, *Nano Lett.*, 2018, **18**, 4493–4499.
23 A. Fumega and V. Pardo, *et al.*, *J. Phys. Chem. C*, 2019, **123**, 27802–27810.
24 P. Coelho, K. Nguyen Cong, M. Bonilla, S. Kolekar, M. H. Phan, J. Avila, M. C. Asensio, I. I. Oleynik and M. Batzill, *J. Phys. Chem. C*, 2019, **123**, 14089–14096.
25 R. Chua, J. Yang, X. He, X. Yu, W. Yu, F. Bussolotti, P. K. J. Wong, K. Loh, M. B. H. Breese, K. J. Goh, Y. Huang and A. T. S. Wee, *Adv. Mater.*, 2020, **32**, 2000693.
26 P. Wong, W. Zhang and F. Bussolotti, *et al.*, *Adv. Mater.*, 2019, **31**, 1901185.
27 D. O'Hara, T. Zhu, A. Trout, A. S. Ahmed, Y. K. Luo, C. H. Lee, M. R. Brenner, S. Rajan, J. A. Gupta, D. W. McComb and R. K. Kawakami, *Nano Lett.*, 2018, **18**, 3125–3131.
28 K. Bronsema and G. Wiegers, *Mat. Res. Bull.*, 1987, **22**, 1073–1080.
29 K. N. Wood and G. Teeter, *ACS Appl. Energy Mater.*, 2018, **1**, 4493–4504.
30 D. Gao, Q. Xue, X. Mao, W. Wang, Q. Xu and D. Xue, *J. Mater. Chem. C*, 2013, **1**, 5909–5916.
31 K. Momma, T. Ikeda, A. A. Belik and F. Izumi, *Powder Diffr.*, 2013, **28**, 184–193.
32 S. Göttlicher and B. Kieselbach, *Acta Cryst.*, 1976, **A32**, 185–192.
33 X. Lu, *et al.*, *Nat. Mater.*, 2015, **14**, 325.
34 X. Fan, *et al.*, *Phys. Rev. Mater.*, 2019, **2**, 114802.
35 N. D. Mermin and H. Wagner, *Phys. Rev. Lett.*, 1996, **17**, 1133–1136.
36 L. Onsager, *Phys. Rev. [Sect.] B*, 1944, **65**, 117–149.
37 N. C. Frey, H. Kumar, B. Anasori, Y. Gogotsi and V. B. Shenoy, *ACS Nano*, 2018, **12**, 6319–6325.